Large-eddy simulation of a compressor rotor

By J. Joo†, G. Medic†, D. A. Philips‡ AND S. T. Bose‡

Wall-modeled large-eddy simulation is applied to a transonic axial compressor rotor (NASA Rotor 37). The simulation results show a significant improvement over fully turbulent RANS in the prediction of the overall performance, mainly by capturing boundary layer transition on the blade. Sensitivity of the result to the end-wall boundary conditions (isothermal/adiabatic walls) and the inflow profile has also been demonstrated.

1. Introduction

For a computational fluid dynamics (CFD) tool to be used reliably in the design of turbomachinery, it must be able to predict the overall performance of a turbomachinery row, as well as the span-wise profiles downstream of it, with a sufficient level of accuracy so that a comparison can be made between different designs. In other words, it has to be accurate enough to allow a designer to recognize which geometrical changes to the design lead to improved performance and which do not; this remains a challenge for conventional RANS simulations. These often erroneously predict the flow field, in particular at off-design conditions, because RANS turbulence closure models perform poorly with flow separation, secondary flow features, and tip-gap vortex capturing. In addition, there is a growing recognition that the fully turbulent flow assumption of conventional models is not correct in turbomachinery, and not including laminar-to-turbulent transition in the computations taints the predictions, even for the design condition.

Large eddy simulation (LES) is an attractive alternative because it can predict transition and separation, and many LES studies have reported successful results throughout the turbomachinery CFD community (Tucker 2013). However, the cost of wall-resolved LES can be prohibitively high; a three-dimensional geometry with a chord-based Reynolds number ranging from several hundred thousands to over one million requires hundreds of millions to several billion grid points for a single sector. Because of fewer restrictive resolution requirements in the turbulent boundary layers, wall-modeled LES is a tractable alternative.

The present investigation performs a wall-modeled LES of a transonic, axial rotor (NASA Rotor 37). Extensive test data is available in Suder (1996), and many computational studies have been carried out since then (Chima 1998, 2009; Hah & Loellbach 1999; Hah 2009; Yamada *et al.* 2003; Ameri 2010; Gomar *et al.* 2011). Most studies inaccurately predicted the overall performance – by missing 3 to 4 percentage points of adiabatic efficiency, as well as the downstream profile shapes which are important in order to capture the intra-row interactions. Chima (1998); Hah & Loellbach (1999) discussed the effect of tip-clearance and large hub corner separation, but the reasons for gaps between the predictions and the test data were not determined conclusively.

Transition to turbulence on the blade surface is another critical feature of Rotor 37. In prior wall-resolved LES investigations of turbomachinery flows, it was found that

† United Technologies Research Center
‡ Cascade Technologies Inc.

	methodology	total grid size	wall $\Delta y+$	inflow profile	solver
Case A	RANS	1.1M	< 1	Profile data	UTC flow solver
Case B	RANS tripped	1.1M	< 1	Profile data	UTC flow solver
Case C	WM LES	11M	~ 50	Plug-flow	CharLES
Case D	WM LES	48M	~ 12	Profile data	CharLES

TABLE 1. Description of computational cases

significant portions of the blade boundary layers were laminar (Medic & Sharma 2012; Medic *et al.* 2015). This study focuses on assessing the ability of wall-modeled LES to accurately predict the rotor blade transition.

Fully turbulent RANS and tripped RANS (trip locations based on mean pressure gradients in order to account for transition) simulations were also performed in addition to the wall-modeled LES. The three approaches are assessed based on their prediction of overall performance/efficiency, secondary flow, and tip-leakage flow.

2. Computational Methodology

The flow solver used for LES calculations is the unstructured compressible flow solver, CharLES, developed at Cascade Technologies, Inc. Details for the numerical discretization can be found in Khalighi *et al.* (2010, 2011); Bres *et al.* (2012, 2013). The Vreman model (Vreman 2004) is used for the sub-grid scale model of LES, and an integral constrained equilibrium wall model is employed. For shock capturing, a hybrid central-ENO scheme was used (Shi *et al.* 2002; Harten *et al.* 1983), accompanied by a shock sensor to identify the discontinuity (Hill & Pullin 2004). The corresponding RANS simulations are conducted by using an in-house UTC flow solver, which is based on a second-order-accurate numerical method for compressible flow equations first presented in Ni (1982), and uses block-structured grid topology. The core of the current solver has been extensively validated for turbomachinery flows over the past 30 years. Steady RANS simulations in this study used the k-ω two-equation turbulence model.

All the cases calculated in this study are tabulated in Table 1.

2.1. *Case set-up*

The computational domain includes one blade sector which covers 10° in the circumferential direction, and extends axially 2 in. upstream and 4 in. downstream from the leading edge, as shown in Figure 1. In the same figure 70% and 95% constant spans and several axial lines are also co-plotted; this information will later be used for post-processing and comparison to data. Detailed geometry information can be found in Suder (1996). At 100% speed (17188.7 RPMs), relative tip and hub Mach numbers are 1.48 and 1.13, respectively. Chord and relative velocity based Reynolds number at 70% span is about 1.3×10^6.

For the block-structured RANS solver, a grid topology with 3 blocks was used: H-mesh, O-mesh, and H-mesh for the flow passage, near the blade region, and the tip-gap region, respectively. The total number of grid points is about 1.1 million. The grid sizes in the stream-wise, pitch-wise, and span-wise directions are 217, 48, and 112 respectively, and the wall normal grid size of the first cell next to the wall is less than 1 in viscous wall units.

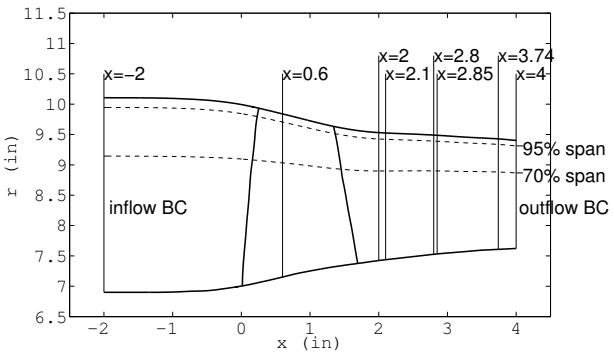

FIGURE 1. A cross-section of the computational domain of NASA Rotor 37 simulations; also included are axial and spanwise cross-sections that are used for comparison with the experimental data.

The grid for LES is constructed by using the local refinement tool, Adapt (developed at Cascade Technologies Inc.), starting from the grid used for RANS. Near-wall grid size is adjusted so that the first cell size is approximately 50 in viscous wall units. Further refinement near the boundary layer and wake regions makes the total grid size 11 million cells.

After the initial LES run, it was found that the wall normal resolution inside the boundary layer on the blade is not adequate – only 4-5 cells are accommodated if the wall $\Delta y+$ of 50 is used. So the wall normal grid size is refined such that the wall $\Delta y+$ is about 12, and 12-15 cells reside inside the boundary layer on the blade. Additional resolution was also provided to capture the shock and to resolve the shock-boundary layer interaction resulting in a 48M cell mesh.

For the inflow conditions, a constant condition without profile information was used for the initial LES case such that the total pressure is 101,350 Pa and the total temperature is 288.15 K, which are representative of the ambient conditions of the test facility. A more realistic condition was then imposed for the refined LES case (the same inflow profiles were used for all RANS simulations).

The velocity profile from the data (Suder 1996) was used to construct a total pressure and temperature profile for the inlet. The core region is assumed to have the total pressure of the sea-level standard day condition, 101,350 Pa, and then uniform static pressure is applied across the inlet. As a result, the mass averaged total pressure becomes 100,286 Pa, which is about a one percent loss from the ambient. Regarding total temperature, a constant value of 288.2 K was used for the total temperature, assuming that there is no work input through the inlet duct.

The end-wall turbulence is generated by a digital filtering technique (Klein *et al.* 2003). The peak value of the turbulent kinetic energy inside the boundary layer is $0.0062U_0$, where U_0 is the center line velocity at the inlet. This peak value in wall units is estimated to be about 3.5. Outside the boundary layer, the turbulent intensity, u/U_0 is about 0.15%, which is representative of typical low disturbance level in such a facility.

The LES was integrated for approximately 6 flow through times to remove the initial transient, and flow statistics were sampled for approximately 6 flow through times thereafter for the coarse LES. The solution for the coarse LES was interpolated onto a refined mesh, and results shown for the refined case were sampled over 2 flow through times.

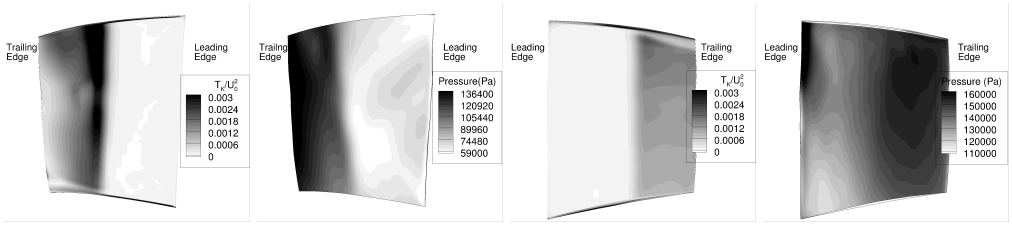

(a) (b) (c) (d)

FIGURE 2. Illustration of trip location for case B; (a) turbulent kinetic energy contours on the plane near the suction surface, (b) static pressure contours on the suction surface, (c) turbulent kinetic energy contours on the plane near the pressure surface, (d) static pressure contours on the pressure surface; $W_C \sim 20.04$ kg/s.

2.2. *Manual tripping in RANS*

Given that much of the rotor blade boundary layer is laminar, the RANS calculations can be manually tripped at predetermined locations by deactivating the RANS model prior to this location. For the tripped RANS simulations, the location of the trip is based on the pressure gradient so that the turbulence model is triggered where the adverse pressure gradient prevails – in particular near the shock location (Figure 2). The turbulence model is active over the entirety of the blade surface in the fully turbulent RANS calculations.

3. Results and discussion

3.1. *Overall performance*

Most important in design analysis is the overall performance: efficiency, pressure ratio, and temperature ratio. Figure 3 shows speed-lines (multiple operating points at the same speed) for RANS and tripped RANS. The LES calculations, cases C and D, appear as predictions of a single operating point. The definitions and computing procedures for performance quantities follow those presented in Suder (1996).

In terms of efficiency, LES and tripped RANS results are distinctly higher than RANS; but, they still under-predict the data as shown in Figure 3(a). Figure 3 highlights the role of the transition on the blade as having a first-order impact on the performance and indicates the need for transition capturing high fidelity simulation or accommodation of the transition in RANS simulation.

In Figure 3(c) a sharply higher total temperature ratio overall computed with LES and tripped RANS implies substantial differences in the flow field when compared with the fully turbulent RANS. From the Euler equations it follows that the higher total temperature means more turning of flow by the compressor blade. As will be discussed below, the transition impacts the shock and boundary layer interaction, the resulting blockage, and ultimately the flow turning, which leads to a significant impact on the performance.

In Figure 3(b) LES and tripped RANS also have a higher overall total pressure ratio, which is consistent with higher predicted-total temperature ratio. However, the total pressure rises less efficiently, so this efficiency is not as high as shown in the data. The impact of thermal boundary conditions on the rotor blade is discussed below in the context of overall efficiency.

The mass flow condition for which the simulations are compared with the data is W_C – corrected mass flow of 20.57 kg/s. Abundant test data is available in Suder (1996).

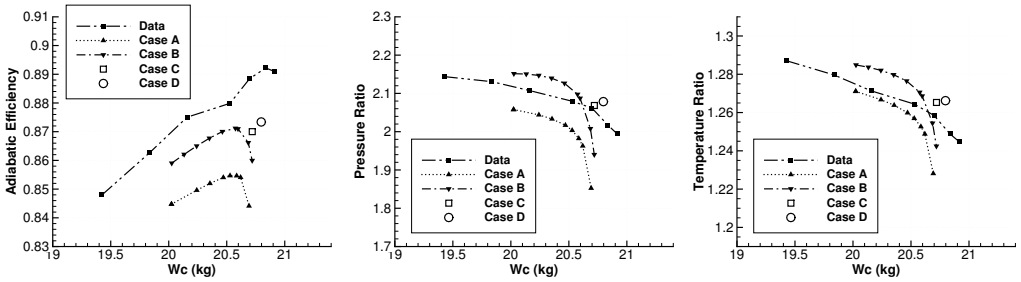

(a) (b) (c)

FIGURE 3. Overall performance curves; (a) efficiency, (b) total pressure ratio, (c) total temperature ratio.

Note that the definition of the corrected flow W_C is

$$W_{corr} = \frac{W\sqrt{\frac{T_{inlet}}{T_{ref}}}}{\frac{P_{inlet}}{P_{ref}}}, \tag{3.1}$$

where P and T are the total conditions and P_{inlet} and T_{ref} are 101350 Pa and 288.2 K respectively.

Unfortunately, the two LES calculations – cases C and D – do not match this condition exactly. The outlet static pressure should be adjusted to correctly match the flow, but the back pressure stated earlier was maintained because of computational cost considerations in order to obtain better converged statistics (adjusting the back pressure requires acoustic waves to traverse the domain several times before a statistically stationary state is reached). However, the key features are well represented and the condition is close enough to be compared with the data.

The radial profiles of total pressure ratio, total temperature ratio, and efficiency at the exit are plotted in Figure 4. Overall, LES calculations show good agreement with the data, although the initial LES (case C) has no inflow profile. This has a significant impact on end-wall flow features and is discussed below.

These profiles lead to a number of observations are investigated in the next sections. In Figure 4(a,b) case A, fully turbulent RANS, look to be shifted back, which is consistent with the overall performance in Figure 3 and it is the result of not accounting for transition. In the same figure RANS simulations, cases A and B, show more undulated profile shape than LES. In Figure 4(b) the LES calculations (and in particular the initial LES, case C) better predict the total temperature ratio near the tip region.

The LES calculation of Hah (2009) predicted the hub corner stall, which is related to the dip of profiles near a 20% span. Our simulations do not predict that feature and so there is an over-prediction of the total pressure under the 30% span. It is not clear what causes the separation – Shabbir *et al.* (1997) argue that it results from the leakage flow from the gap between the rotating and stationary part in the hub whereas Hah (2009) disagrees with that idea, asserting that the hub separation occurs without the leakage flow. However, it should be noted that the number of span-wise grid points of Hah (2009) is 129, which is not enough to resolve end-wall boundary layers. Also, it is not clear how well the inflow profile matched the experimental data; comparison of cases C and D in the current study shows substantial differences in the results that are at least partially from the inflow boundary condition.

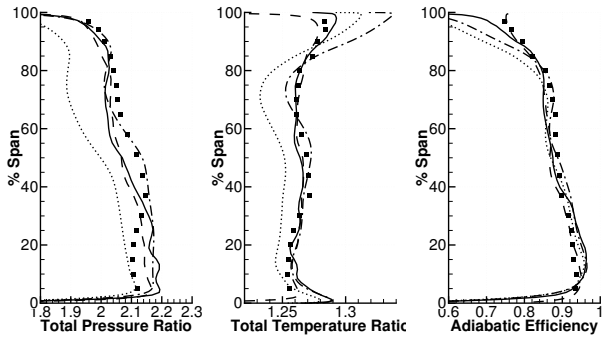

FIGURE 4. Performance profiles at the exit of the computational domain; symbols: data at $W_C \sim 20.57$ kg/s; dotted line: case A – RANS, dash-dot line: case B – tripped RANS, dashed line: case C – the initial LES, solid line: case D – the final LES.

The total temperature in cases A, B, and D is over-predicted near the tip and hub region (Figure 4). When compared with the initial LES (case C) where a flat inlet profile is assumed, the over-prediction in these regions is more pronounced with a realistic profile, highlighting the sensitivity to the inflow condition. As discussed below, appropriate thermal boundary conditions are also needed to be able to accurately predict temperature near the end-walls.

3.2. *Blade loading*

The blade loading at a 70% span is compared with the data for the same corrected mass flow of 20.57 kg/s in Figure 5. Experimental data for pressure coefficient (C_P) presented in Suder (1996) is calculated from the estimated boundary layer edge Mach number via the isentropic relationship. Over the separation bubble, the edge is significantly away from the surface, and the pressure distribution computed this way is different from the surface pressure. The exact procedure to determine the edge Mach number used to process test data is not fully documented, so there are still some potential differences in the processing of the simulation results.

Overall the agreement is reasonable considering the above discussion on post-processing, as well as the slight differences between the operating conditions in computations and the experiment. Note that all simulations predict the shock location somewhat farther downstream than the experimental data indicates. In addition, fully turbulent RANS (case A) under-predicts the overall pressure rise more significantly, as previously illustrated by the results presented in Figures 4 and 5. The refined LES (case D) better captures the pressure rise resulting from the shock compared with the other computations as shown in Figure 5.

3.3. *Transition on the blade*

The experimental setup of Suder (1996) does not utilize a turbulence-generating grid so the compressor operated in a low level of free-stream turbulence, which is unlikely to promote by-pass transition. This is somewhat representative of the conditions in the front rows of high-pressure compressors.

In such an environment, the expectation is that the front of the blade is laminar. Only when the flow experiences an adverse pressure gradient, this will cause either laminar

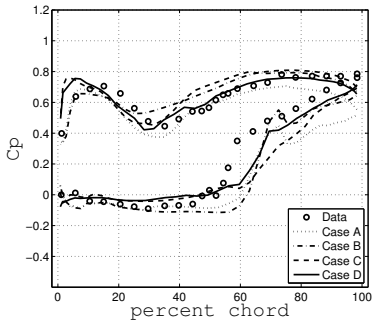

FIGURE 5. Blade loading at a 70% span at $W_C \sim 20.57$ kg/s; Cp is calculated from the edge Mach number.

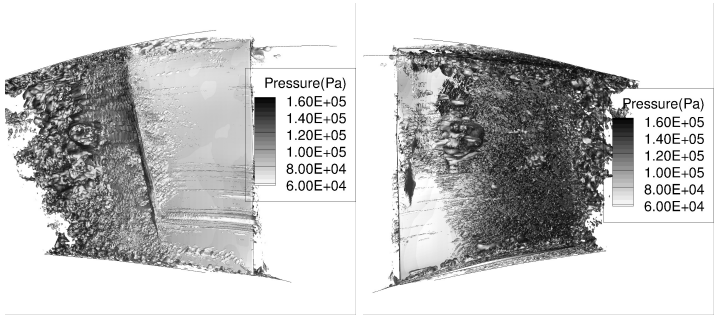

FIGURE 6. Iso-surfaces of $u'/U_0 \sim 0.1$ of case D – the final LES; suction side (left); pressure side (right).

separation or an inflectional velocity profile in the boundary layer. These are both inviscidly unstable and would lead to transition to turbulence. Indeed, Figure 6 showed that the transition is captured for the current LES calculations leaving a significant portion of the blade laminar. Yet, the accuracy of the transition location is difficult to assess with the existing experimental data.

3.4. *Tip-leakage flow*

3.4.1. *Leakage flow and temperature rise*

As shown in Figure 4, the RANS simulations, cases A and B, over-predict the total temperature ratio toward the tip region (as well as near the hub) while the LES cases do not. This over-prediction is a persistent problem (see Suder 1996, Figure 17).

The over-prediction of total temperature in the tip-region is related to the tip-leakage flow. The total temperature contour plots on the plane normal to the axial direction at about 40% of the chord are shown in Figure 7(a-d). The tip-leakage vortex can be delineated by high total temperature spots, and the size of the vortex core corresponds to the amount of the total temperature peak near the tip as shown in Figure 4.

The high total temperature of tip-leakage flow is primarily due to its high static temperature as shown in Figure 7(e-h). The static temperature of the flow has risen behind the shock, and the leakage flow (which already passed through the upstream shock) migrates toward the shock from the neighboring passage. In effect, the tip-leakage flow

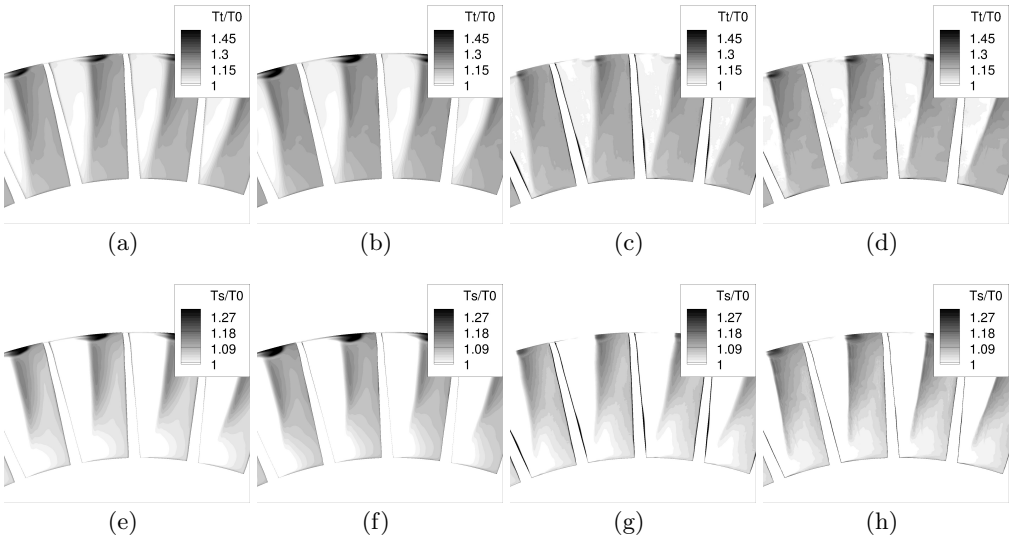

FIGURE 7. Total temperature (upper part) and static temperature (lower part) contours on an axial slice at x=0.6.; (a), (e) case A; (b), (f) case B; (c), (g) case C; (d), (h) case D; the view is looking upstream; the left edge of the blade is the pressure side, the right edge is the suction side; the axial location is indicated in Figure 1.

is heated twice by the shock compression. Temperature ratio near the tip can be an indication of the amount of the leakage flow.

The relative Mach number contours at a 95% span is shown in Figure 8(a-e), where the strength of the leakage flow is compared against measured data. The fully turbulent RANS simulation (case A) shows the best agreement with the experimental data, whereas LES calculations (cases C and D) under-predict its strength. Figure 8(f) provides another measurement for the leakage flow prediction. The low level of the axial momentum of the leakage flow causes the wake defect. Similarly, the fully turbulent RANS simulation (case A) is closest to the data and the LES calculations (cases C and D) under-predict it.

One of the reasons for under-prediction of tip-leakage flow in LES can be attributed to the grid resolution inside the tip gap. The coarse LES has only 6 computational cells in the tip gap and the tip gap resolution is identical between cases C and D. The RANS simulations have 16 cells, which are clustered near the end-wall. Proper resolution of the tip gap is necessary to accurately capture the total temperature, which will be a subject of future investigations.

3.4.2. *Thermal boundary condition*

While the fully turbulent RANS simulation (case A) predicts the right level of leakage flow, Figure 8(f), the total temperature is too high near the tip. For turbomachinery simulations, an adiabatic boundary condition is widely used for the end-wall (often because it is lacking sufficient information about the end-wall temperature). However, the present study shows that it can have a substantial impact on the performance predictions. Note that unless the experimental test section is carefully insulated, there will always be some heat loss.

As a sensitivity study, an iso-thermal boundary condition for the end-wall was tested with two different temperatures. One temperature is taken from the mid-span and mid-

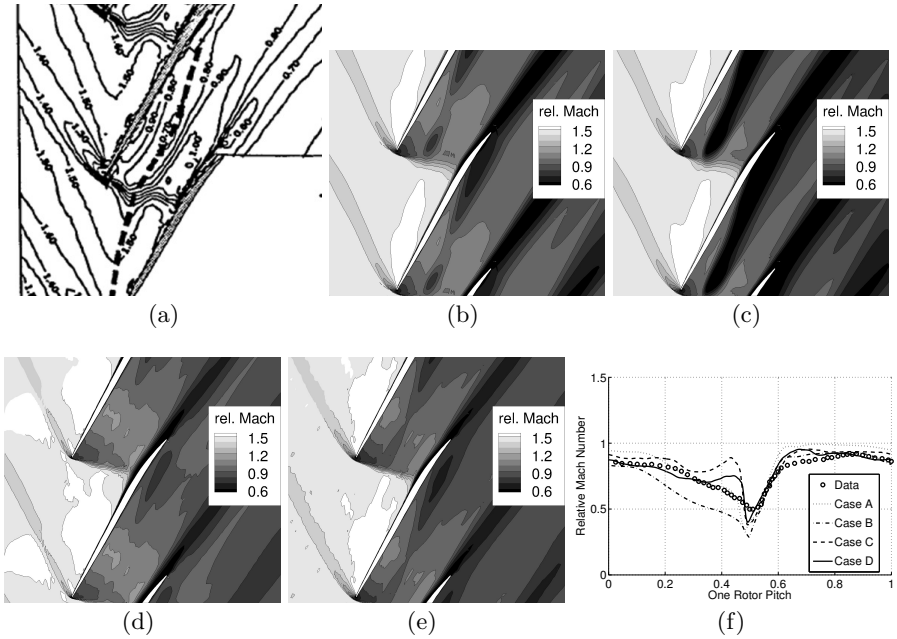

FIGURE 8. Relative Mach number contours at a 95% span; (a) the data, (b) case A – RANS, (c) case B – tripped RANS, (d) case C – the initial LES, (e) case D – the final LES; (f) relative Mach number profile at a 95% span and 4% chord downstream after the trailing edge.

pitch axial distribution of the fluid temperature through the compressor. It undergoes a temperature rise across the shock location; i.e., the resulting wall temperature distribution is a step function. The other temperature is a uniform end-wall temperature that corresponds to an inlet temperature. The actual wall temperature is likely between these two values.

Figure 9(a,b) show strong sensitivity to the thermal boundary condition of the tip and hub total temperature prediction. The total temperature peak of the fully turbulent RANS (case A) falls toward the experimental data when predicted with the wall temperature of mid-span flow. Although there is overall under-prediction of the total temperature, the effect of the leakage flow locally dominates the tip-region. The tripped RANS (case B) still over-predicts the tip temperature ratio as it over-produces the leakage flow as well.

The reduced total temperature near the end-wall, using iso-thermal boundary condition, affects the overall efficiency prediction (simply from its definition). Figure 9(c) shows the range of possible efficiencies predicted by the tripped RANS framework using different thermal boundary conditions. The under-prediction of efficiency in CFD could potentially stem from a misuse of the adiabatic boundary condition, and the sensitivity to the iso-thermal boundary conditions suggests that the heat loss needs to be assessed and properly taken into account.

4. Conclusions and future work

Computational results from wall-modeled LES, fully turbulent and tripped RANS for NASA Rotor 37 are analyzed in detail and compared with the data.

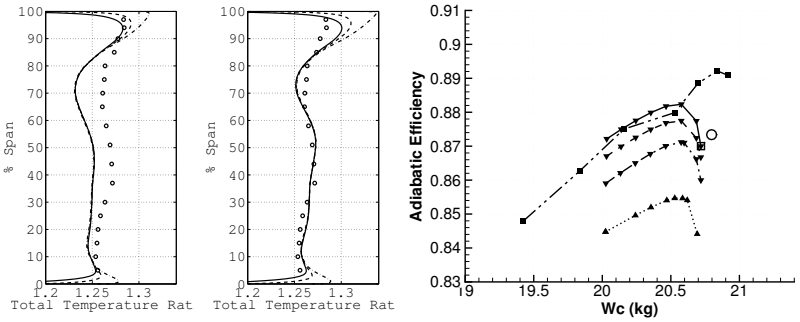

(a) (b) (c)

FIGURE 9. (a)-(b) Total temperature ratio at the exit of the domain with different thermal boundary condition at the end-walls; (a) case A – RANS, (b) case B – tripped RANS; (c) efficiency curves with different thermal boundary condition; dash-dot line: adiabatic; dashed line: iso-thermal, equal to fluid temperature across the compressor at mid-span and mid-pitch; solid line: iso-thermal, equal to inlet fluid temperature.

The wall-modeled LES captures the transition and shows improved prediction of overall performance compared with the fully turbulent RANS. Tripped RANS simulations show a similar trend, confirming the importance of accounting for transition on the blade surface for accurate predictions of the overall performance. The reason for this improvement stems mainly from the difference in predicted size of the separation region after the shock and boundary layer interaction. In addition, LES calculations also predict more accurately the wake and mixing losses.

The LES calculations, however, under-predicted tip-leakage flow, likely because of inadequate grid resolution, whereas RANS simulations captured the tip-leakage more accurately. The tip-leakage flow has higher static temperatures and leads to an over-prediction of the total temperature ratio near the tip. This can potentially be attributed to the use of an adiabatic boundary condition for the end-walls; a sensitivity study with iso-thermal boundary conditions showed a reduction of this over-prediction.

Acknowledgments

The authors wish to thank Professor Parviz Moin and the Center for Turbulence Research at Stanford University for their hospitality and technical support. The extra efforts of supporting CharLES and executing simulations by Cascade Technologies Inc. are gratefully acknowledged.

REFERENCES

AMERI, A. A. 2010 *NASA Rotor 37 CFD code validation - Glenn-HT code.* NASA Technical Report no. CR-2010-216235.

BRES, G. A., HAM, F. E., NICHOLS, J. W. & LELE, S. K. 2013 Nozzle wall modeling in unstructured Large Eddy Simulations for hot supersonic jet predictions. *AIAA Paper 2013-2142*.

BRES, G. A., NICHOLS, J. W., LELE, S. K. & HAM, F. E. 2012 Towards best practices for jet noise predictions with unstructured Large Eddy Simulation. *AIAA Paper 2012-2965*.

Chima, R. V. 1998 Calculation of tip clearance effects in a transonic compressor rotor. *J. Turbomach.* **120**, 131–140.

Chima, R. V. 2009 *Swift code assessment for two similar transonic compressors.* NASA Technical Report no. TM-2009-215520.

Gomar, A., Gourdain, N. & Dufour, G. 2011 High fidelity simulation of the turbulent flow in a transonic axial compressor. In *Euro. Turbomach. Conf.*. Istanbul, Turkey.

Hah, C. 2009 *Large Eddy Simulation of transonic flow field in NASA rotor 37.* NASA Technical Report no. TM-2009-215627.

Hah, C. & Loellbach, J. 1999 Development of hub corner stall and its influence on the performance of axial compressor blade rows. *J. Turbomach.* **121**, 67–77.

Harten, A., Lax, P. & Van Leer, B. 1983 On upstream differencing and godunov-type schemes for hyperbolic conservation laws. *SIAM Rev.* **15**, 35 -61.

Hill, D. J. & Pullin, D. I. 2004 Hybrid tuned center-difference-weno method for Large Eddy Simulations in the presence of strong shocks. *J. Comput. Phys.* **194**, 435–450.

Khalighi, Y., Ham, F., Moin, P., Lele, S. K., Colonius, T., Schlinker, R. H., Reba, R. A. & Simonich, J. 2010 Unstructured Large Eddy Simulation technology for prediction and control of jet noise. In *Proc. of ASME Turbo Expo 2010*.

Khalighi, Y., Nichols, J. W., Ham, F., Lele, S. K. & Moin, P. 2011 Unstructured Large Eddy Simulation for prediction of noise issued from turbulent jets in various configurations. *AIAA Paper 2011-2886*.

Klein, M., Sadiki, A. & Janicka, J. 2003 A digital filter based generation of inflow data for spatially developing direct numerical or Large Eddy Simulations. *J. Comput. Phys.* **186**, 652–665.

Medic, G. & Sharma, O. 2012 Large Eddy Simulation of flow in a low-pressure turbine cascade. In *Proc. of ASME Turbo Expo 2012*.

Medic, G., Zhang, V., Wang, G., Tang, G.and Joo, J. & Sharma, O. P. 2015 Prediction of transition and losses in compressor cascades using Large Eddy Simulation. In *Proc. of ASME Turbo Expo 2015*.

Ni, R.-H. 1982 A multiple-grid scheme for solving the euler equations. *AIAA J.* **20** (11), 1565–1571.

Shabbir, A., Celestina, M., Adamczyk, J. & Strazisar, A. 1997 The effect of hub leakage flow on two high speed axial compressor rotors. In *ASME Paper 97-GT-346*.

Shi, J., Hu, C., & Shu, C. 2002 A technique of treating negative weights in weno schemes. *J. Comput. Phys.* **175**, 108–127.

Suder, K. 1996 *Experimental investigation of the flow field in a transonic, axial flow compressor with respect to the development of blockage and loss.* NASA Technical Report no. TM-107310.

Tucker, P. 2013 Trends in turbomachinery turbulence treatments. *Prog. Aerospace Sci.* **63**, 1–32.

Vreman, A. 2004 An eddy-viscosity subgrid-scale model for turbulent shear flow: Algebraic theory and applications. *Phys. Fluids* **16**, 3670–3682.

Yamada, K., Furukawa, M., Inoue, M. & Funazaki, K. 2003 Numerical analysis of tip leakage flow field in a transonic axial compressor rotor. In *8th Int. Gas Turbine Cong.*